Stepping stones in CO2 utilization

Towards process development of oxalic and glycolic acid monomers

Schuler, E.

Publication date
2022

IV

Wenn man die Fragen lebt, lebt man vielleicht
– ohne es zu merken –
in die Antworten hinein.

- Rainer Maria Rilke -

Superbases as catalysts in formate to oxalate coupling

Chapter IV

Superbases as catalysts in the formate to oxalate coupling reaction

Abstract An interesting contribution to solving the climate crisis involves the use of CO_2 as a feedstock for monomers to produce sustainable plastics. In the European Horizon 2020 project "OCEAN" we develop a continuous multistep process from CO_2 to oxalic acid and derivatives, starting with the electrochemical reduction of CO_2 to potassium formate. The subsequent formate to oxalate coupling is a reaction that has been studied and commercially used for over 150 years. With the introduction of superbases as catalysts under moisture-free conditions, we now show unprecedented improvements for the formate coupling reaction. With isotopic labelling experiments, we prove the presence of carbonite as an intermediate during the reaction and with a unique Operando set-up, we studied the kinetics. Ultimately, we were able to drop the required reaction temperature from 400 °C to below 200 °C, reduce the reaction time from 10 minutes to 1 minute whilst achieving 99% oxalate yield. .

4.1 Introduction

Formate coupling to oxalate is an old reaction first discovered in 1852 and was the main commercial way to produce oxalic acid before the advent of petrochemical routes. [1–3] With the ambition of the society to decrease atmospheric CO_2 levels, the Carbon Capture and Utilization (CCU) approach to produce chemicals from CO_2 is receiving significant interest. [4–10] Commercially, the formate to oxalate coupling reaction (FOCR) is performed at high temperatures of 380-420°C using hydroxides as catalysts. [11–14] With these hydroxide bases, the reaction takes more than 30 minutes to proceed, but reaction temperatures are high and oxalate yields are not optimal. Especially the production of carbonate as a side product is problematic as it requires the introduction of a downstream separation step. The reaction kinetics as a function of process conditions was extensively studied in the 1930s in Russia by Freidlin. [15–27] In the 1970-80s Shishido and Gorski investigated the coupling reaction focusing on the decomposition products and the reaction mechanism. [28–33] Recently, the FOCR as part of CCU pathways gained new interest and several new patents and studies were published in China. [34–45] A recent publication on the topic was from Lakkaraju e*t al.* who introduced hydrides as catalysts and presented a new mechanism. [46] Our work was initially sparked by the many questions still open after reading the previous publications. We explored alternative catalysts, mainly the superbases (SB) such as Lithium-, Sodium- and Potassium Hydride as well as Sodium Amide (NaH, KH, LiH and $NaNH_2$), optimized the reaction conditions, studied kinetics and mechanisms and found an optimal alternative process for the FOCR.

4.2 Methods

All reactions were performed in a purposely built reactor which can be operated using variable temperature gradients or pre-heated and reaches 700°C. Glass-vials with a volume of 15 mL were used as reactors at temperatures from 25 - 450°C. The reactions were performed in the Argon atmosphere without purging but pressure relief via a vent port. The experimental series included reaction time, temperature, heating rate, catalyst type and catalyst loading as variables to understand mechanistic differences and find the catalysts delivering the highest yield at the lowest temperature in the shortest time possible. All chemicals were reagent grade and obtained from Sigma-Aldrich. Sample preparation included drying of all reagents in a vacuum oven and introduction to an argon-filled glove box at oxygen and water levels below 0.1 ppm. All catalyst and formate mixtures were prepared in 5 g batch sizes by meticulous mixing using a mortar and pestle. Kinetic measurements were performed using an Operando Raman spectrometer coupled with a purpose build bubble counting device for high-resolution gas quantification. [47] Quantitative analysis of solid products was performed by liquid-cell IR and LC measurements.

4.3 Results and Discussion

In the quest of finding new catalysts that can decrease the reaction temperature and time, we first tried to understand the FOCR reaction better, by looking at the probable mechanism. Many reaction mechanisms have been proposed and most recently

Lakkaraju *et al.* suggested carbonite (COO^{2-}) as the key intermediate species as shown in Scheme 4.1. [46]

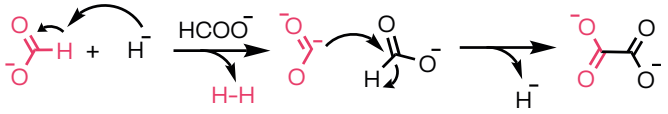

Scheme 4.1 FOCR promoted by base catalysts with carbonite as intermediate as suggested by Lakkaraju et al. [46]

This is an interesting study from the mechanistic point of view, however, no significant improvements in terms of selectivity, reaction time and reaction temperature were reported. We first tried to follow the reaction with Raman spectroscopy (see Figure 4.1A). However, we were not able to see the carbonite peak at any given configuration. We then used isotope labelling studies. With an excess catalyst, the carbonite lifetime increases due to reduced formate (reaction partner) concentration, as shown with Raman studies by Lakkaraju *et al.* We first produced carbonite by adding an excess amount of hydride. The carbonite prevails as it doesn't find a reaction partner. We then introduced D_2O as a reaction partner, which reacted with carbonite to form deuterated formate ($DCOO^-$; see Scheme 4.2). The reaction was quenched after completion. The only species observed in a GC-MS (with electrospray ionization) of the quenched sample had a m/z of 46 corresponding to deuterated formate ($DCOO^-$). We also did two control reactions: (1) quenching the reaction with water (2) adding D_2O to formate without performing the coupling reaction. In both cases, we observed 45 m/z corresponding to formate ($HCOO^-$).

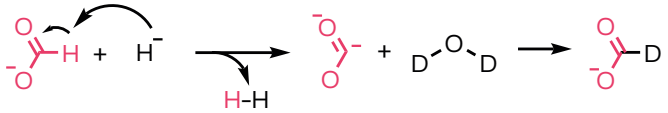

Scheme 4.2 Reaction pathway for isotope labelling of Carbonite intermediate with D_2O.

The formation of the carbonite being the rate-limiting step explains the need for a strong base to extract the proton from the formate ($HCOO^-$) anion. Their catalytic activity relies on their intrinsic property of strong basicity and not on complex molecular or surface structures such as in respectively homogeneous or heterogeneous catalysts. Based on this insight, we tested compounds well known for their basic properties and compared them to hydroxides, the state-of-the-art catalyst since 1882. [48,49] We did these tests under inert conditions using home-build high-speed kinetic measurement equipment based on the work of Slot *et al.* connected with Operando Raman spectroscopy and gas analysis capabilities. [47]

Our results shown in Table 4.1 indicate that four catalysts, LiH, NaH, KH and $NaNH_2$, show excellent activity due to their superbase properties. These catalysts are superior in oxalate yield and allow the reaction to proceed 10 times faster at temperatures 200°C lower than that used with hydroxides. The catalysts gave yields of up to 97%, with reaction occurring soon after melting of the substrate (169°C) and going to completion in 1 to 3 minutes.

For all catalysts the reactions were performed at varying temperatures and the achieved oxalate yields, as measured by both LC and IR, are shown in Figure 4.1B. Without a catalyst, the reaction starts at 360 °C, reaching yields of up to 21% at 420 °C – however, the required reaction time as shown in Figure 4.1D exceeds 3 hours.

Hydroxide catalyst speeds up the reaction to 30 minutes and lowers the required reaction

temperature to 410 - 430 °C. Early patents for batch processes report even longer times of up to 6 hours. [50–53] When reacting potassium formate with hydroxide bases, only 63 % oxalate yield could be achieved. The reduced yield can partly be explained by side reaction (1) and product decomposition reaction (2) towards carbonate.

$$HCOOK + KOH \rightarrow K_2CO_3 + H_2 \quad \text{Eq. (1)}$$

$$K_2C_2O_4 + 2\,KOH \rightarrow 2\,K_2CO_3 + H_2 \quad \text{Eq. (2)}$$

The yields with our superbase catalysts are very high at 99% but are not higher than the literature values reported with sodium formate as a reactant; however, the rate of the reaction is higher and the reaction temperature is much lower. [25,46] Moreover, no formation of carbonate as a side-product was observed with our superbase catalysts and the reaction follows a zero-order regime throughout. The confirmed presence of carbonite when SBs were used supports the Lakkaraju mechanism but our observation that the reactions proceed at 200°C lower temperatures emphasizes the importance of absolute moisture and oxygen-free reaction environment. In the presence of (small amounts) of water, the hydrides (present at low concentrations) are converted to hydroxides, requiring conventional reaction temperatures (300-400°C). We also noticed the dependency of oxalate yields on counter-ions as well as reactor designs. We are currently investigating this dependency and will report mechanistic reasons as well as solutions in upcoming publications.

Table 4.1 Performance indicators of catalysts for coupling of potassium formate

Catalyst	Reaction onset temp. (°C)	Ideal reaction temp. (°C) [a]	Oxalate yield (%) [b]	Reaction time (min) [c]
NaH [d]	350	380 – 420	99	10
NaH	153	180 - 200	95	0.5 - 2
KH	153	180 - 200	97	1 - 2
LiH	153	180 - 200	95	1 - 2
$NaNH_2$	154	180 - 200	95	< 1
$NaBH_4$	320	335 - 360	88	5 - 15
KOH	327	410 - 430	63	10 - 30
uncatalyzed	360	420 - 440	21	150 - 200

[a] Temperature at which highest yields were achieved [b] Highest yield achieved with 2.5 wt.% catalyst loading [c] Time at which 90% conversion was achieved [d] Reference from Lakkaraju et al. using Sodium Formate and NaH as a catalyst. The reaction was observed at 350 °C. No observation of reaction-start at the melting point of formate. [46]

When using a temperature profile starting at 25 °C and heating at 1 °C min^{-1}, the reaction starts from a low temperature (~ 153 °C) for the superbases and reaches maximum rate around the melting of formate (169 °C). The fast reaction upon melting and similar behaviour of all SBs, despite their difference in basicity, suggest the possibility of even lower reaction temperatures, if the melting temperature could be lowered. This would be one of the future directions to study.

Strong foaming through the hydrogen evolution during the vigorous start of the reaction causes solidification of the product as a foamed-up structure (shown in Figure 4.S4). This fast reaction doesn't give enough time for efficient mass transfer and mixing and thereby encapsulates some unreacted formate. Therefore, adequate mixing of the reactant and catalyst for example by milling is important as the reaction proceeds quickly upon melting.

In our set-up, temperatures of 200 °C were required to achieve the maximum yield.

Below this temperature, the conversion was not complete and proceeded slower as shown in Figure 4.1C. Moreover, the heating rate is also of great importance as it can significantly influence the oxalate yield.[32] Slower heating rates of 0.25 °C min^{-1} to 2 °C min^{-1} ensure better gas escape through the reactant particles and prevent the puffing,

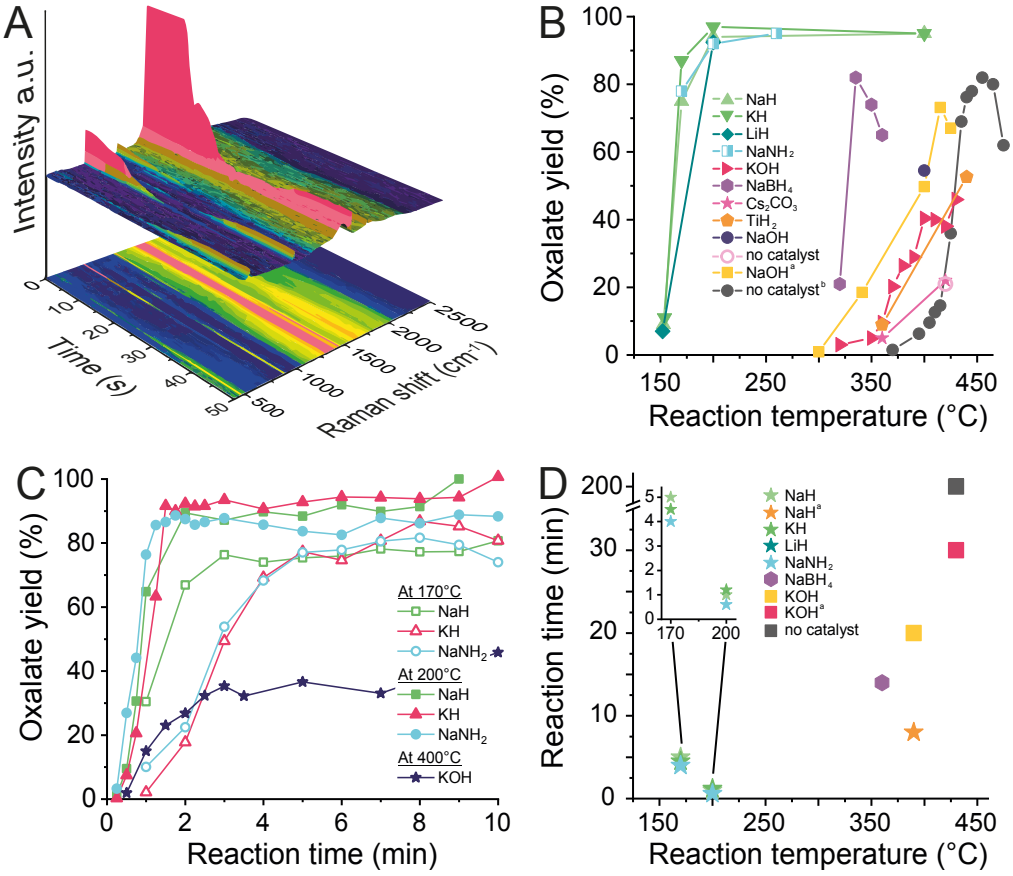

Figure 4.1 A Time-resolved Raman spectrum from formate coupling reaction using 10 wt.% NaH at 200 °C in a pre-heated reactor. The first ten seconds are not shown as they represent the heat-up time of the reactor. The peaks at 770, 1084, 1342, 1364 and 1532 cm^{-1} can be attributed to formate. These disappear within 25 seconds after which peaks of Oxalate appear at 467, 881, 1437 and 1617 cm^{-1}. The peak indicative of carbonite at 1076 cm^{-1} did not appear during or after the reaction. **B** The oxalate yields at different reaction temperatures for the potassium formate coupling reaction are plotted for all tested catalysts accompanied by two literature values. Each data point represents a single experiment at the given temperature in a pre-heated reactor and not temperature profiles. In the end, the oxalate yield was determined by IR and LC measurements. SB catalysed reactions showed great improvements in yield at low temperatures. [a] Sodium formate with sodium hydroxide values from Freidlin *et al.*[25] [b] Non-catalysed potassium values from Freidlin *et al.*[21] **C** Oxalate yields obtained with instantaneous heating in the pre-heated reactor, each data point represents an individual reaction quenched after the given time. Higher oxalate yields in FCR with SBs are obtained faster at 200 °C compared to reactions at 170 °C (melting of reactant). However, Hydroxide catalysed FCR is much slower even at 400 °C. **D** The dependency of reaction times on the reaction temperature is shown. All reaction times correspond to the point when >90% conversion was reached. Higher temperatures and stronger bases reduce the reaction times drastically by up to 200-times compared to non-catalysed reactions and 30-times compared to the conventional KOH catalyst. [a] Values reported by Lakkaraju *et al.*[46]

leading to a tightly packed product at the bottom of a reaction vial with a high yield at 170 °C (Figure 4.S4). However, this comes with the consequence of longer residence times for reaction completion.

Although inert conditions in the absence of oxygen are important to prevent oxidative side reactions to carbonates for FOCR in general, the absolute absence of water is crucial for SBs. The presence of water leads to decomposition reactions as in Scheme 4.3, losing the advantage of superbase.

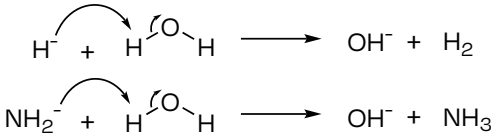

Scheme 4.3 Hydride and amide ion reaction with water leading to catalyst transformation to hydroxide (and deactivation).

The minimum catalyst required for the reaction is hence heavily influenced by the dryness of the reactor and reactants. At our small scale (290 - 310 mg of substrate per experiment) we needed a minimum catalyst loading between 0.05 wt.% and 0.2 wt.% which can be attributed to varying amounts of moisture remaining in the substrate. With loadings above 1 wt.%, the reaction proceeded at its maximum speed for all SBs. Unlike hydroxides, there are no side reactions when using SBs and consequently, no carbonate or any other side-product was observed for temperatures up to 450 °C. Above 450 °C oxalate decomposes to carbonate and CO. However, these temperatures are never required for the reactions with SBs.

Metal hydrides such as TiH_2, MgH_2 and $NaBH_4$ are commonly used for hydrogen storage. We tested them as catalysts for the FOCR but did not observe catalytic activity for TiH_2 and MgH_2 and slightly higher activity for $NaBH_4$ compared with KOH. Metal hydrides with two hydrogen atoms attached are more stable (less basic) and more importantly do not release hydride ions, which are crucial for the reaction. Consequently, they do not catalyse the reaction. The fast liberation of hydrogen seen in Figure 4.S6 does not reflect formate conversion as it originates from the metal hydrides. Borohydrides are also widely used in organic chemistry as a reducing agent. Their thermal stability and high basicity make them a promising candidate for the reaction. We indeed see catalytic activity starting at 285 °C with the highest yields reached at 335 °C. Above this temperature, the reaction proceeds faster but the yield drops with increasing temperature. We attribute this to the decomposition of the borohydride which also destroys the formed oxalate by reactive borohydride or boron species. During the decomposition of $NaBH_4$ also a lot of hydrogen is released, which explains the surplus production as shown in Figure 4.2C compared to the expected value obtained from FOCR alone.

The suitability of caesium carbonate as a base capable of proton abstraction was proposed by Banerjee et al. [54] Using it in our FOCR experiments however showed no activity beyond the self-catalysed reaction as shown in Figure 4.S6. Caesium carbonate is a weaker base compared to hydroxides and thus its proton abstraction qualities are expected to be worse.

Our kinetic experiments are based on high-resolution bubble counting (example reactions shown in Figure 4.2A and 4.2B, set-up shown in Figure 4.S3) connected with Operando Raman measurements. For calculations of rate, reaction order and activation energies we used the hydrogen volumetric data due to its high resolution (2000 bubbles per minute)

with a total number of 5000 gas bubbles for each experiment. With non-isothermal kinetic experiments in the range of 25-450 °C, Figure 4.2C shows the respective reaction rates and Figure 4.2D shows the turnover frequencies (TOF) as calculated using Eq. S11 (low performing catalysts are shown in Figure 4.S6). The reaction rates for SBs exceed non-catalysed and hydroxide catalysed reactions by a factor of 5 and borohydride catalysed reactions by a factor of 2. Sodium amide shows the highest turnover frequency followed by sodium and potassium hydrides. Lithium hydride had a low TOF which was caused by the fast reaction combined with a relatively higher catalyst loading. Caesium carbonate and MgO only show minor improvements in the reaction rate relative to the uncatalyzed reaction. For TiH_2 the hydrogen release coincides with the reaction start and causes a falsely high measured reaction rate.

We used Arrhenius plots to calculate the activation energy and pre-exponential factor A as shown in Table 4.2 (also more data shown in Table 4.S1). A is often referred to as the "frequency" factor and indicates the rate at which molecular collisions occur and therefore indicative of the contribution of a physical effect on the reaction or if the calculated activation energies are purely chemical activation values. If A is larger than 10^{30} s^{-1} physical diffusion limitation of the reaction is likely. [55]

Table 4.2. Performance indicators of catalysts for the formate coupling reaction.

Catalyst	Activation energy (kJ mol^{-1})	Pre-exponential factor A (s^{-1})	Error (± kJ mol^{-1})
NaH	527	3.02×10^{67}	5.68
KH	535	4.18×10^{67}	5.54
LiH	814	6.54×10^{86}	11.1
$NaNH_2$	305	3.90×10^{56}	25.5
$NaBH_4$	266	1.09×10^{23}	-
KOH	125	1.06×10^{13}	-
HCOOK	196	1.28×10^{19}	-

The calculated activation energy for the FOCR without a catalyst is 196 kJ mol^{-1} and agrees with literature values. [56] The low pre-exponential factor of 1.28 x 10^{19} s^{-1} points to an absence of physical effects. Lower activation energies are expected when catalysts are used. For KOH we calculated activation energy of 125 kJ mol^{-1} and A equals 1.06×10^{13} s^{-1}.

So far, only Lakkaraju *et al.* estimated the activation energy for a catalysed FOCR using sodium formate as the reactant. They used the Eyring-Polanyi equation which gave activation energy of approximately 177 kJ mol^{-1} and a pre-exponential factor A of 1.3 x 10^{37} s^{-1}. This indicates that their activation energy entails physical effects which explains also the relatively high number – especially as they claim to have used hydrides. However, they required a temperature range between 330 and 420 °C – a typical range for hydroxide catalysed reaction, which is far above the melting point of 253 °C for the sodium formate. The increased activation energy and reaction temperature suggest that hydride was not the active species in their reactions.

In our experiments, hydrides and amides performed better at lower temperatures than hydroxides and thus even lower activation energies were expected. However, the calculated energies are up to 5 times higher than for the hydroxide catalysed reaction (between 330-546 kJ mol^{-1} ± 5.6 kJ mol^{-1}; Table 4.2 and Table 4.S1; plots in Figure 4.S5). The values are independent of catalyst loading and are high, from 3.90×10^{56} s^{-1} to 6.54

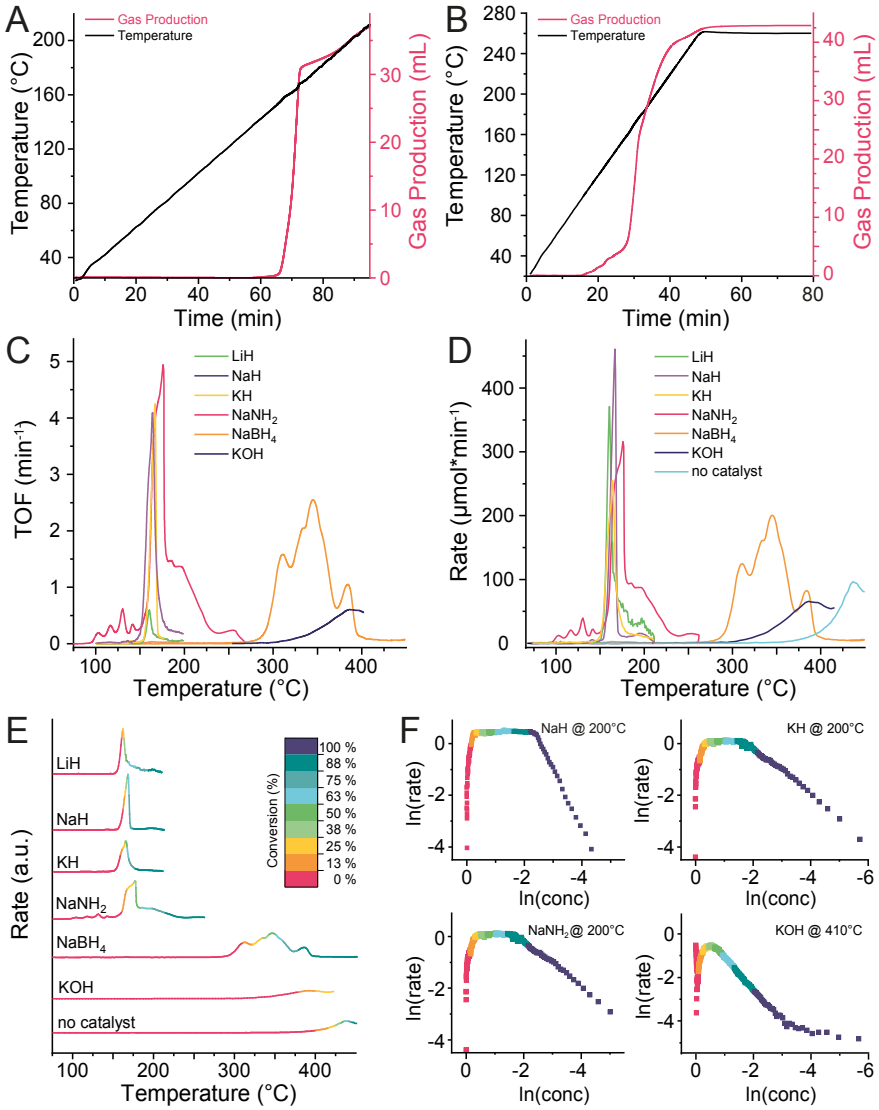

Figure 4.2. A Kinetic graph was obtained in a bubble counter experiment for 1 wt.% NaH catalysed reaction with potassium formate. During the reaction, the temperature is increased at a constant rate of 2 °C min^{-1}. As a measure of reaction progress, the gas production from the reaction is measured using a Bubble-Counter. The gas volume expected for full conversion of all formate to oxalate is approximately 40 mL **B** Kinetic experiment similar to A when using 2.5 wt.% $NaNH_2$ as catalyst instead. **C** Reaction rates for reactions at various catalyst loadings with respect to the temperature which is increased at a constant rate of 2 °C min^{-1}. The drop of the reaction rate at increasing temperature especially for SBs originates from the completion of the reaction. We are unable to provide rate data for higher temperatures as the reaction rate exceeds the physically possible heating rate of the mixture. Sodium borohydride marks an exception and has other, yet unknown, side reactions happening. **D** Turnover frequencies for all successful catalysts were calculated based on the reaction rate and the catalyst loading with respect to the temperature which is increased at a constant rate of 2 °C min^{-1}. **E** Reaction rates for different catalysts at different conversion stages. It becomes apparent that the reaction rate drops as expected when the reaction reaches full conversion. This is only not the case for $NaBH_4$, KOH and the non-catalysed reaction which cause gas production due to decomposition. **F** The logarithm of gas production during the isothermal reaction is plotted against the change in formate concentration to evaluate the reaction order. For reactions, I, II, and III a horizontal part of the graphs corresponds to 0 reaction order (from yellow to light blue). The slope in IV is 1 as observed also for the other reactions towards full conversion (blue to dark blue).

$\times 10^{86}$ s^{-1}. Together with the observed coincidence of reaction onset and melting, this indicates the dominance of physical processes. These include the endothermic melting of formate, strong diffusion upon melting, mass transfer limitations from the immediate formation of solid product and heat loss with the produced gas. Non-isothermal kinetic experiments in the same set-up revealed that SB reactions follow zero-order kinetics, which is in contrast to first-order behaviour observed for hydroxide catalysed reactions.

Figure 4.2F illustrates that this zero-order reaction is observed throughout 75% of the reaction and then slows down to first-order behaviour - except for NaH catalysed reactions which change towards second-order behaviour. The zero-order reaction indicates that a truly catalytic reaction is present and the maximum reaction rate is reached due to the strong excess of reactant over the catalyst. With the reaction progress, limited mass transfer due to the formation of solid oxalate occurs.

The first-order behaviour of hydroxide catalysed reactions indicates a dependency on reactant concentration. The Hydroxide reaction requires the in-situ generation of reactive hydride and therefore has a more complex mechanism, which we are studying now. True activation energies of the SB catalysed reactions require a separation of the physical effects from the reaction start. This can be achieved when melting occurs before the start of the reaction or when operating in a solvated system. Stirring improves mass transfer and optimal reactant mixing whilst no energy liberated by melting obstructs the measurement. To achieve this, we tried to create eutectic salt mixtures with lower melting points; we determined their melting points with differential scanning calorimetry. However, we did not observe any significant drop in the melting temperature (see also Figure 4.S7).

4.4 Conclusions

In conclusion, we report significant improvements in reaction rates of formate coupling at low temperatures using superbase catalysts. We also obtained mechanistic and kinetic insights for the reaction with isotope labelling and operando kinetic studies. We identify that reactant mixing, absence of H_2O and O_2, inert atmosphere and slow heating are important for getting high yields with a rapid rate at low catalyst loadings. This is the first time, a significant reduction in the reaction temperature of FOCR (from 380-420 to 170-200 °C) is reported. Additionally, the reaction times are reduced from 5 - 10 minutes to 0.5 - 2 minutes whilst achieving oxalate yields of 99%. Catalyst loadings as little as 0.01 wt.% proved effective and in contrast to hydroxide catalysed coupling, no carbonate was formed as a side product. Among several superbase catalysts tested, alkali metal hydrides, amides and borohydrides proved suitable whilst alkaline and transition metal hydrides did not work. We detected high reaction rates for reactions catalysed with SBs compared to traditional hydroxide catalysts. SB catalysed FOCRs were shown to follow zero-order behaviour in contrast to hydroxide and non-catalysed FOCRs. Activation energies for non-catalyzed and hydroxide catalysed FOCRs were measured and were found to agree with the literature. However, we could not estimate the true chemical activation energies for SB catalysed reactions. The kinetics of new SB catalysed reactions are mainly determined by physical processes such as substrate melting and

mixing of reactants – the true chemical activation energies could not be determined, as illustrated by the very high pre-exponential factors obtained. However, the results are very reproducible, also for the physical effects and are independent of the catalyst concentration. Open questions will be addressed in an upcoming publication using experimental and computational techniques (Molecular dynamics).

Concerning the commercial application of our SB based system, the lower reaction temperature, shorter residence time and the elimination of downstream separation are beneficial. Yet, the handling of superbases is more critical compared to hydroxides as the requirement of oxygen- and moisture-free conditions add an energy-intensive formate pre-drying. Similar to the case of hydroxide catalysts, hydride catalyst recovery is not essential. At 1% catalyst loading, the hydride catalyst cost is only a marginal part of the overall oxalic acid production cost. At larger scales, we also expect a further reduction of the hydride catalyst amount. Overall, our results deepen significantly the mechanistic understanding of the FOCR and potentially allow for a better and more sustainable process. Moreover, our work will help accelerate the development of new processes starting from CO_2-derived formates as carbon sources.

References

1 Jullion; Crane; MacDougall; Rawson. Polytech. J., 1852, 124 (42), 175–181.

2 Laber, G. In Ullmanns Enzyklopadie der technischen Chemie, Wiley-VCH Verlag GmbH & Co. KGaA: Weinheim, 1962, Vol. 13, pp 51–55.

3 Florio, P. A. In Kirk-Othmer Encyclopedia of chemical technology, second edition, Interscience Publishers, 1967, Vol. 14, pp 356–373.

4 Bollen, J. In Designing Sustainable Technologies, Products and Policies, Springer International Publishing: Cham, 2018, pp 307–309, DOI:10.1007/978-3-319-66981-6_33.

5 Aresta, M. Carbon Dioxide as Chemical Feedstock, Aresta, M., Ed., Wiley, 2010, DOI:10.1002/9783527629916.

6 Putting CO2 to Use - Creating Value from Emissions, Paris, 2019.

7 Styring, P.; Quadrelli, E. A.; Armstrong, K. In Carbon Dioxide Utilisation: Closing the Carbon Cycle: First Edition, Elsevier, 2015, pp 237–272, DOI:10.1016/C2012-0-02814-1.

8 Raza, A.; Gholami, R.; Rezaee, R.; Rasouli, V.; Rabiei, M. Petroleum, 2019, 5 (4), 335–340, DOI:10.1016/j.petlm.2018.12.007.

9 Gnanakumar, E. S.; Chandran, N.; Kozhevnikov, I. V.; Grau-Atienza, A.; Ramos Fernández, E. V.; Sepulveda-Escribano, A.; Shiju, N. R. Chem. Eng. Sci., 2019, 194, 2–9, DOI:10.1016/j.ces.2018.08.038.

10 Ronda-Lloret, M.; Rothenberg, G.; Shiju, N. R. ChemSusChem, 2019, 12 (17), 3896–3914, DOI:10.1002/cssc.201900915.

11 Riemenschneider, W.; Tanifuji, M. In Ullmann ' s Encyclopedia of Industrial Chemistry, Wiley-VCH Verlag GmbH & Co. KGaA: Weinheim, 2012, Vol. 25, pp 529–541, DOI:10.1002/14356007.a18.

12 Setton; R. Bull. soc. chim. Fr., 1958, Vol: No. 11-12.

13 Meurs, J. H. H. WO2016/124646A1, 2016.

14 Kaczur, J. J.; Lakkaraju, P. P.; Parajuli, R. R. WO2017121887A1, 2017.

15 Freidlin, L. K.; Balandin, A. A.; Lebedeva, A. I. Russ. Chem. Bull. (Izvestiya Akad. Nauk SSSR), 1941, 2, 275–288.

16 Freidlin, L. K. Zhurnal Obs. Khimii, 1937, 7 (11), 1675–1683.

17 Freidlin, L. K.; Balandin, A. A.; Lebedeva, A. I. Russ. Chem. Bull. (Izvestiya Akad. Nauk SSSR), 1941, 2, 268–274.

18 Freidlin, L. K. Trans. All-Union Acad. Food Ind. named after Stalin, 1939, No. 10, 145–157.

19 Freidlin, L. K. Sci. reports Moscow Univ., 1936, 152–156.

20 Freidlin, L. K.; Balandin, A. A.; Lebedeva, A. I. Bull. acad. sci. U. R. S. S., Cl. sci. math. nat., Ser. chim., 1940, 6, 955–962.

21 Freidlin, L. K. Promyshlennost Org. Khimii, 1937, 3, 681–686.

22 Freidlin, L. K. Zhurnal Prikl. Khimii, 1938, 11 (6), 975–980.

23 Balandin, A. A.; Freidlin, L. K.; Vaskevich, D. N. Sci. Repts. Moscow State Univ., 1936, 6 (No. 6), 321–345.

24 Freidlin, L. K.; Balandin, A. A.; Lebedeva, A. I. Russ. Chem. Bull. (Izvestiya Akad. Nauk SSSR), 1941, 2, 261–267.

25 Freidlin, L. K. Zhurnal Prikl. Khimii, 1937, 10 (6), 1086–1094.

26 Freidlin, L. K.; Balandin, A. A.; Lebedeva, A. I. Russ. Chem. Bull. (Izvestiya Akad. Nauk SSSR), 1941, 2, 255–262.

27 Balandin, A. A.; Freidlin, L. K. Zhurnal Obs. Khimii, 1935, 6 (6), 868–872.

28 Shishido, S.; Masuda, Y. Nippon Kagaku Kaishi, 1976, 5 (46), 325–1675, DOI:10.1246/nikkashi.1976.66.

29 Shishido, S.; Masuda, Y. Nippon Kagaku Kaishi, 1973, No. 1, 185–188, DOI:10.1246/nikkashi.1973.185.

30 Górski, A.; Kraśnicka, A. J. Therm. Anal., 1987, 32 (4), 1243–1251, DOI:10.1007/BF01905178.

31 Górski, A.; Kraśnicka, A. D. J. Therm. Anal., 1987, 32 (4), 1229–1241, DOI:10.1007/BF01905177.

32 Górski, A.; Kraśnicka, A. D. J. Therm. Anal., 1987, 32 (7), 1895–1904, DOI:10.1007/BF01913982.

33 Górski, A.; Kraśnicka, A. D. J. Therm. Anal., 1987, 32 (5), 1345–1354, DOI:10.1007/BF01913334.

34 Yu, X. CN1502599A, 2004.

35 Xie, K. CN1727322A, 2006.

36 Xu, Z.; Cheng, X.; Xia, W. CN102391099A, 2012.

37 Guo, Q. CN107216248A, 2017.

38 Ma, Q.; Li, A.; Li, Y. CN100999462A, 2007.

39 Li, A.; Li, Y. CN1927805A, 2007.

40 Li, A.; Liu, C.; Li, Q. CN101077855A, 2007.

41 Cao, Z.; Cao, Y. CN201343509Y, 2009.

42 Cao, Z.; Cao, Y. CN101462943A, 2009.

43 Li, A.; Li, Y. CN101823950A, 2010.

44 Jiang, H.; Li, D.; Jiang, Z.; Wang, D.; Ban, Z.; Zhang, B. CN102659556A, 2012.

45 Li, A.; Li, Y.; Zhao, Z.; Zhang, A.; Li, Z. CN1903821B, 2012.

46 Lakkaraju, P. S.; Askerka, M.; Beyer, H.; Ryan, C. T.; Dobbins, T.; Bennett, C.; Kaczur, J. J.; et al. ChemCatChem, 2016, 8 (22), 3453–3457, DOI:10.1002/cctc.201600765.

47 Slot, T. K.; Shiju, N. R.; Rothenberg, G. Angew. Chemie Int. Ed., 2019, 58 (48), 17273–17276, DOI:10.1002/anie.201911005.

48 Merz, V.; Weith, W. Berichte der Dtsch. Chem. Gesellschaft, 1882, 15 (2), 1507–1513, DOI:10.1002/cber.18820150215.

49 Goldschmidt, M. US659733, 1900.

50 Wiens, A. US714347, 1902.

51 Andrews, L. W. US1281117, 1918.

52 Enderli, M.; Schrodt, A. US2033097, 1936.

53 Hene, E. US2004867, 1935.

54 Banerjee, A.; Kanan, M. W. ACS Cent. Sci., 2018, 4 (5), 606–613, DOI:10.1021/acscentsci.8b00108.

55 Goldstein, B.; Levine, H.; Torney, D. SIAM J. Appl. Math., 2007, 67 (4), 1147–1165, DOI:10.1137/060655018.

56 Hartman, K.; Hisatsune, I. C. J. Phys. Chem., 1966, 583 (2), 1281–1287.

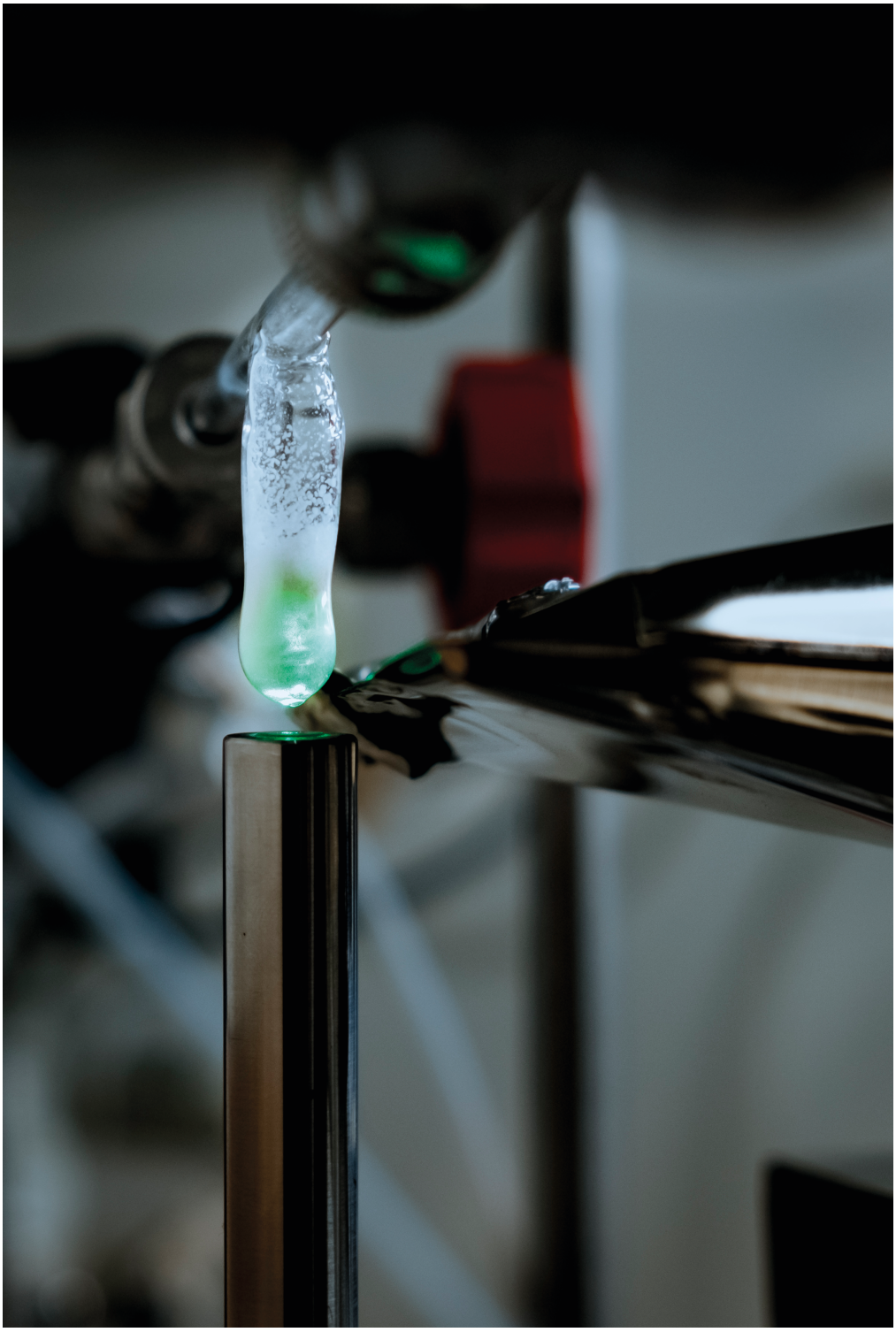

Picture above First steps with the Raman set-up in Tarragona, Eric Schuler, 2018

Chapter 4: Supporting information

S4.1 Experimental details

4.4.1 Reagents

All chemicals (Potassium formate, Sodium formate, Potassium oxalate, Sodium formate, Potassium hydride, Sodium hydride, Lithium hydride, Sodium amide, Potassium hydroxide, Sodium borohydride) were obtained from commercial suppliers (Sigma-Aldrich®), dried and stored in a dry environment. Otherwise, the chemicals were not further processed.

S4.1.1 Sample preparation

Potassium and sodium formate were dried overnight in a vacuum oven at 110 °C and transferred to the glove box. Hydride catalysts were transferred to the glove box directly and washed with dry hexane if needed to remove the protective wax film and subsequently dried under vacuum. Reaction mixtures for catalyst screening were prepared in batches of different wt.% ratios of catalyst to formate. For each batch, 3-5 g of dry potassium sodium formate or potassium oxalate were crushed in a ceramic mortar until a fine powder was obtained. After 5 minutes of mixing the batch was transferred to a glass vial with a plastic septum cap. The different weight loadings of catalyst (0.01, 0.5, 1, 2.5, 5, 10, 25 wt.%) were weighed and mixed with the formate. The standard batch size was 5 g to reduce weighing error. For each reaction, 290-310 mg of the mixture was used. The exact mass was measured and used to calculate theoretical yields of produced gases and solids. The samples for oxalate decomposition were prepared following the same procedure.

S4.1.2 Kinetic measurements

The kinetics of the reactions were studied by time-resolved volumetric measurements of the produced gas during the reaction. This was performed with a self-build digital kinetic evaluation device called 'Bubble-Counter' and was first described in 2019.[1] This device was invented by Thierry Slot (HIMS, UvA) and is capable of measuring gas production over time (so-called "bubble counting") and heating of the sample using an internal PID loop. Each gas bubble is recorded as a string of values. The gases are subsequently qualitatively analyzed using MS or GC. The string includes the time when the bubble was counted, its bubble size and the corresponding temperature value of a thermocouple. The thermocouple can be placed on the heating element or inside the reactor. This way the reaction can be studied in a broad temperature range with high time resolution.

For all experiments, 7 mL glass vials were used as reactors in a ring-shaped heating element connected to the PID controller in the "Bubble-Counter" device.

S4.1.3 Non-isothermal measurements

For non-isothermal measurements, the reaction vial was ramped to a setpoint temperature with either 0.2 °C min^{-1}, 2 °C min^{-1} or 5 °C min^{-1} heating rates. For reactions at lower temperatures with NaH, KH, LiH, and $NaNH_2$ the reaction vessel was heated from room temperature to 210 °C with the same ramping rate. For higher temperature

reactions using KOH or $NaBH_4$ as catalyst reaction was ramped from room temperatures to 420 °C. After holding the sample for 20 min at the reached temperature, the reactor was taken out and cooled to room temperature. The remaining catalyst was then quenched with 1 mL of distilled water.

S4.1.4 Isothermal experiments

For isothermal experiments, the heating element was preheated to the desired reaction temperature. Each reactor was inserted in the heating element and taken out with 15-60 s intervals between the samples. After the reaction, samples were immediately quenched in the ice bath, weighed inside the glove box and quenched with 1 mL of distilled water.

S4.1.5 Oxalate decomposition

For the decomposition reaction of oxalate, the reaction mixture was heated to 450 °C with a heating rate of 5 °C min^{-1}.

S4.2 Calculations of reaction kinetics

S4.2.1 Reaction order

To estimate the reaction, order the formulas beneath were used. The reaction order is defined as a dependence of the rate of a chemical reaction on the concentrations of the reactants. [2]

For formate coupling this can be written as:

$$rate = k * [Formate]^n \quad \text{Eq. (S1)}$$

Where k and n are the reaction rate constant and reaction order for the formate concentration.

To experimentally determine the reaction, order the following formulae can be implemented:

$$(observed)\ rate = k * [reactant]^n \quad \text{Eq. (S2)}$$

Taking the natural log of both sides of the equation (Eq. S2) gives:

$$\ln(rate) = \ln\left(k * [reactant]^n\right) \quad \text{Eq. (S3)}$$

After rearrangement:

$$\ln(rate) = \ln(k) + n * \ln([reactant]) \quad \text{Eq. (S4)}$$

Now if one plots ln(rate) vs. ln([reactant]), using (Eq. S4), the resulted graph should look like a linear function. The slope of the graph accounts for the reaction order. From the intercept, one can derive a rate constant of the reaction k. [3]

S4.2.2 Activation energy

To determine the activation energy one can use the linear logarithmic form of the Arrhenius equation:

$$\ln(k) = \ln(A) - \frac{a}{R} \times \frac{1}{T} \quad \text{Eq. (S5)}$$

It uses the dependency of a logarithm of reaction constant k on the reciprocal temperature. Plotting the ln k against 1/T produces a straight line. The slope represents the activation energy, whilst the intercept leads to the pre-exponential factor A. This pre-exponential factor is often referred to as "frequency" factor A and indicates the rate at which molecular collisions occur. [2]

S4.2.3 Turnover frequency

To determine the turnover frequency at a specific reaction temperature, the intrinsic molar reaction rate is corrected by the amount of catalyst present during the reaction. The amount of catalyst present is expressed in molar loading :

$$\mathrm{TOF} = (\text{Intrinsic rate (mol/s)})/(\textit{catalyst loanding}\ (\textit{mol})\ ) \qquad \text{Eq. (S6)}$$

4.4.2 Calculation in practice

Table 4.S6.1 Paramters for kinetic calculations based on Slot *et al* [1]

Parameter	Name	Source / Calculations
1	Time (min)	Raw data
2	Beam interruption time (BIT units)	Raw data
3	Volume (µL)	Raw data
4	Volume, blank subtracted (µL)	Raw data
5	Temperature (°C)	Raw data
6	Time Interpolation (min)	50 point Interpolation of X=**1**, Y=**4**, X data
7	Volume Interpolation (µL)	50 point Interpolation of X=**1**, Y=**4**, Y data
8	Temperature interpolation (°C)	Interpolation of X=**6** in (X=**1**, Y=**5**), Y data
9	Observed rate (µL)	Derivate of (X=**6**, Y=**7**), against time
10	Fractional conversion (0-1)	1 – (**7** / maximum expected volume)
11	Intrinsic rate (µL/min)	**9** / ((1-**10**)^n) n = reaction order = 1 for formate coupling
12	Observed rate (M/min)	**9** / constant, depending on stoichiometry of the reaction and molar concentration
13	Intrinsic rate (M/min)	**11** / constant, depending on stoichiometry of the reaction and molar concentration
14	1000/T	1000 / (**8**+273.15)
15	ln (k)	ln(**13**)

In practice, we used a spreadsheet to calculate the kinetic reaction parameters which are based on the spreadsheets described by Slot et al.[1] The raw data is imported into the spreadsheet from the ASCII file created by the bubble counter. To obtain an equal spread, the data is first interpolated and the value obtained from volume vs. time is then differentiated. Taking the derivative vs. temperature is not desirable because the temperature ramp rate at the start of an experiment may not be constant in the first 10°C

of the observed range. The fractional conversion during the reaction is calculated from the expected hydrogen production from formate conversion (based on the exact mass of reactant in each experiment).

S4.3 Product Analysis

S4.3.1 Raman spectroscopy

We used a Tornado Hyperflux Pro Raman spectrometer equipped with an Axiom RFP 400 probe and a laser with a 785 nm wavelength. A hole on the bottom of the heating element was used to access the reactor from the bottom during the reaction. A time resolution of 900 ms was realized. During the reaction, also the volume and composition of the gases were analyzed online. We used this system to follow the reaction and further confirm the reaction progression by an additional mean.

S4.3.2 Characterization

Products were characterized using different absorbance bands of oxalate, formate, and carbonate in FTIR spectroscopy. To ensure high-quality results, random samples were double-checked with liquid chromatography and ion chromatography. The produced gases were determined by mass spectrometry and gas chromatography. ^{1}H NMR and ^{13}C NMR spectroscopy were implemented to confirm molecular structures and the presence of intermediates. Isotope labelling, combined with mass spectrometry was used to identify possible carbonite intermediate. Raman spectroscopy was used to identify possible reaction mechanisms and follow the reaction time-resolved spectroscopically.

S4.3.3 Quantitative and qualitative IR analysis

We used a SmartSeal liquid cell from PIKE technologies with CaF_2 windows and a cavity thickness of 0.025 mm. The spectra were recorded with a Varian 660-IR spectrometer. The exact analysis theory, procedure and calculations are described in the supporting information of chapter 3 (S3.2.1 and S3.2.2)

S4.3.4 Liquid chromatography

For product analysis with liquid chromatography, the dissolved samples were diluted with purified water to a maximum salt concentration of 1 mg/mL. We use an internal standard and an Agilent 1200 series HPLC with a diode array detector.

S4.3.5 Mass spectrometry

To study the gas species evolving from the formate coupling reactor online we used a Pfeiffer Vacuum Omnistar GSD 330 01 to analyze the off-gases of the reactor.

Mass spectra for the mechanistic studies were collected on an AccuTOF LC, JMS-T100LP Mass spectrometer (JEOL, Japan). For these measurements, reaction products were quenched with deuterium oxide (D_2O) instead of deionized water. It was expected that formed carbonite ions – if any – after quenching with D_2O will transform into deuterated formate. Deuterated formate could be observed at different mass to charge ratios in the MS spectrum. The measurement conditions in the mass spectrometer for Positive

and Negative-ion mode were: Needle voltage 2500 V, Orifice 1 voltage 120 V, Orifice 2 voltage 9 V, Ring Lens voltage 22 V. Orifice 1 80 °C, Desolvating Chamber 250 °C. Flow injection with a flow rate of 0.01 mL/min. All mass spectra were recorded with an average duration of 0.5 min.

S4.3.6 Gas chromatography

We use an Agilent 7820A GC system equipped with Hayesep Q and a Molecular sieve 5A column to analyse the gases originating from the formate coupling reactions. Both online measurements and cumulative measurements with a mix of all produced gases were performed.

S4.3.7 Nuclear magnetic resonance

NMR spectra were recorded on a Bruker AMX 300 (300.1 MHz and 75.5 MHz for ^{1}H and ^{13}C respectively) and Bruker AMX 400 (400.1 MHz and 100.6 MHz for ^{1}H and ^{13}C respectively).

S4.3.8 Differential scaling calorimetry

Differential scanning calorimetry (DSC) measurements were used to determine the melting points of the reaction mixtures. A Mettler Toledo DSC 3+ was used with aluminium crucibles. The samples were prepared in the glove box to prevent contact with moisture. Samples were tested for melting points in a range from 25 to 300 °C at a heating rate of 1 °C/min.

S4.4 Details on mechanistic investigations

S4.4.1 Isotopic labelling experiments

For the isotope labelling experiments we performed a potassium formate coupling reaction with hydrides in excess (e.g. 10 wt.% NaH). After completion of the reaction, the solid mixture was quenched with D_2O. The remaining carbonite in the solid then reacts with the D_2O to form deuterated formate. As standards, we also added D_2O to dry potassium formate and the potassium formate/hydride mixture without performing the reaction. The liquid samples were analyzed using AccuTOF LC, JMS-T100LP Mass spectrometer with electrospray ionization as described above. For deuterated formate ions, we expect an m/z value of 46. For conventional formate, we expect an m/z value of 45. Oxalate, which is present in the sample after reaction, is expected to be unstable with ESI due to the proximity of the charges in the molecule.

The major Peak in the mass spectrum for the quenched formate coupling reaction was 46 m/z, indicating the sole presence of deuterated formate as shown in figure S1. None of the control experiments showed the presence of a 46 m/z signal, but a signal at 45 m/z.

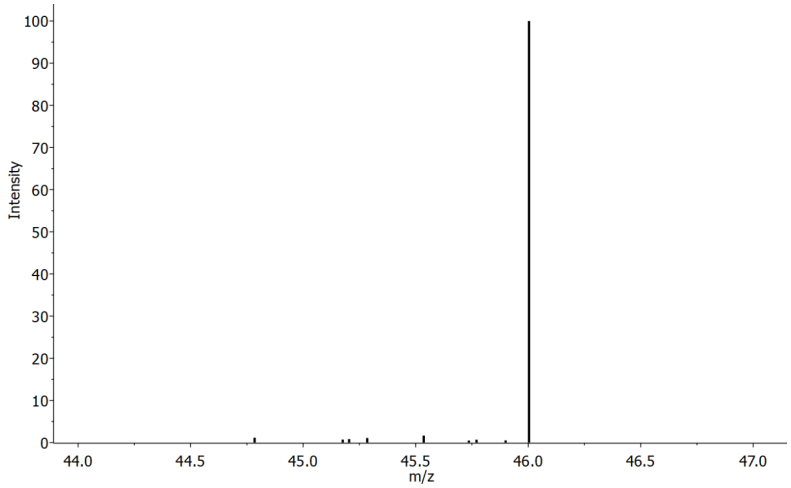

Figure 4.S1 Mass spectrum of deuterium labelled formate after the reaction. The peak at 46 m/z is indicative of deuterated formate ($DCOO^-$). No non-labelled formate ($HCOO^-$) with 45 m/z was observed in the sample.

S4.5 Details on reaction kinetics

S4.5.1 Operando Raman experiments

We follow the reaction by time-resolved Raman over the full reaction time. The conversion of formate to oxalate can be observed. The Carbonite signal which was seen by Lakkaraju et al. could not be observed in any of our many attempts.[4] The figure below shows the set-up:

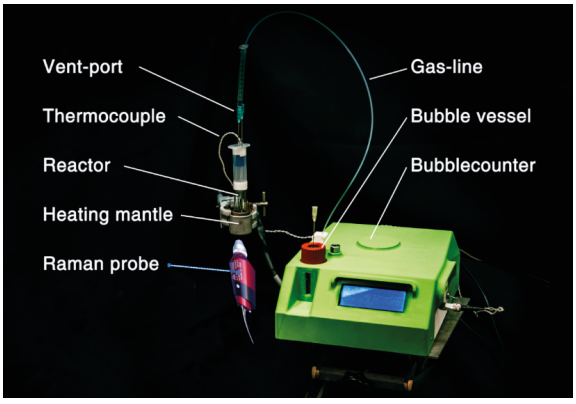

Figure 4.S2 The bubble counter coupled with operando Raman set-up for mechanistic and kinetic experiments. The bubble counter both counts produced gas bubbles and controls the heating mantle. Reactor and bubble vessel are connected via a gas line; inert conditions are kept as the bubble vessel functions as an airlock.

S4.5.2 Foaming during the formate coupling reaction

The physical structure of the reaction product depends on the heating rate of the reaction. We tested different heating rates and in figure S3 below the compact solid, achieved with slow heating rates, and puffed up structure, resulting from fast heating rates. Are shown.

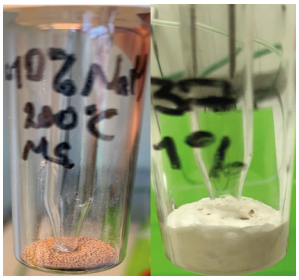

Figure 4.S3 With slow heating at 0.5 °C/min the product forms a compact solid (left). With fast heating in a pre-heated reactor at 200 °C, a puffed-up foam was obtained (right).

S4.5.3 Activation energies obtained from kinetic experiments

The activation energies were calculated for various potential reaction orders and different catalyst loadings. The full list of calculated activation energies, errors and pre-exponential factors are presented below.

Table 4.S1 Activation energy and pre-exponential factors for formate coupling using different catalysts.

Catalyst	Catalyst Loading (wt. %)	Activation energy (kJ mol^{-1})				Temperature range (onset Temp) (°C)	Pre-exponential factor A (s^{-1})	Error (± kJ mol^{-1})
		Observed rate	Intrinsic rate (k)					
			0 order	1 order	2 order			
NaH	0.5	535	535	576	609	157 – 162	5.62×10^{67}	5.68
	1.0	516	516	559	603	157 – 162	1.39×10^{65}	
	2.5	530	530	587	643	157 – 162	2.06×10^{67}	
KH	2.5	546	546	558	576	152 – 155	4.15×10^{68}	5.54
	1.0	527	527	536	544	155 – 160	2.79×10^{66}	
	5.0	534	534	577	619	157 – 162	5.62×10^{67}	
LiH	1.0	831	831	921	1011	161 – 163	7.22×10^{86}	11.1
	5.0	793	793	801	810	152 – 154	9.77×10^{85}	
	10.0	818	818	841	856	153 – 158	2.65×10^{86}	
$NaNH_2$	2.5	330	330	341	355	157 – 162	2.87×10^{56}	25.5
	1	279	279	294	305	155 – 162	4.92×10^{41}	
KOH	5	125	125	129	133	318 – 348	1.06×10^{13}	-
HCOOK	0	196	196	202	208	363 – 409	1.28×10^{19}	-

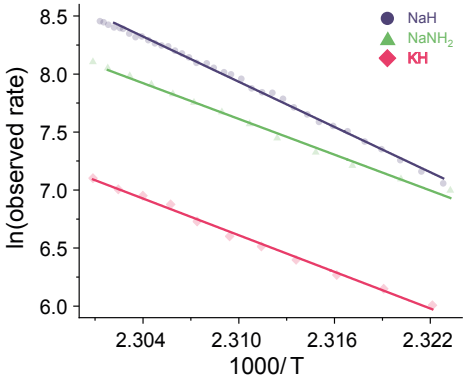

Below you find examples for Arrhenius plots to calculate the activation energies of different formate coupling reactions.

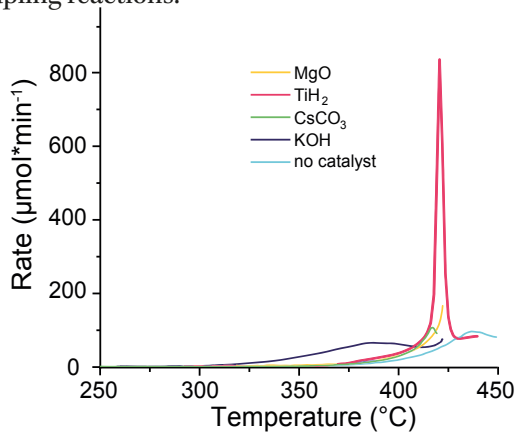

Figure 4.S4 Arrhenius plots for the hydride and amide catalysed reactions. More gas was produced with NaH, indicating that NaH is more active in the formate coupling. $NaNH_2$ showed similar behaviour with lower activation energies.

Figure 4.S5 Rate of Hydrogen evolution during FCR with potassium formate observed with catalysts that showed no catalytic activity.KOH was added as a comparison.

References

1 Slot, T. K.; Shiju, N. R.; Rothenberg, G. Angew. Chemie Int. Ed., 2019, 58 (48), 17273–17276, DOI:10.1002/anie.201911005.

2 Atkins, P.; Paula, J. de. Physical Chemistry, 8th ed., H., F. W., Ed., 2006.

3 Chorkendorff, I.; Niemantsverdriet, J. W. In Concepts of Modern Catalysis and Kinetics, Wiley Online Books, 2007, pp 23–78, DOI:-doi:10.1002/3527602658.ch2.

4 Lakkaraju, P. S.; Askerka, M.; Beyer, H.; Ryan, C. T.; Dobbins, T.; Bennett, C.; Kaczur, J. J.; et al. ChemCatChem, 2016, 8 (22), 3453–3457, DOI:10.1002/cctc.201600765.